On the effect of change in doping concentration and doping radius on the gain of 10% alumina co-doped host-based TDFA

RAJANDEEP SINGH[*], MANINDER LAL SINGH[*]
Department of Electronics Technology, GNDU Amritsar, India

TDFA (Thulium doped optical amplifier) for S-band enables the use of S-band. In this paper, the effect of change in doping parameters on the gain of 10 mol% alumina co-doped TDFA is analyzed for 1050 nm, 1050 nm + 1400 nm, 1050 nm + 800 nm, 1050 nm +1400 nm + 800 nm pumping schemes. The system is analyzed for a doping concentration value of 20×10^{24} m^{-3} and 40×10^{24} m^{-3}, while the doping radius is varied from 0.3 µm to 1.3 µm. A significant effect of the doping parameters on the performance of TDFA is observed. Out of the considered parameters, the highest peak gain of 30.5 dB is observed for the 1050 nm + 1400 nm + 800 nm pumping of the TDFA, which has a doping concentration of 40×10^{24} m^{-3} and doping radius of 0.9 µm. The gain for above mentioned optimum parameters shows the gain enhancement of ~15 dB over the reference case of 1050 nm pumping of TDFA with a doping concentration of 20×10^{24} m^{-3} and a doping radius of 1.3 µm.

1. Introduction

The excellent response of the EDFA (Erbium doped fiber amplifier) is the main reason for the widespread deployment of optical systems operating in C-band [1]–[3]. Apart from EDFA, Raman amplifier, and SOA (Semiconductor optical amplifier) perform well in the C-band [4]–[7]. TDFA is a glass based amplifer which provides gain to S-band signals. On the basis of the glass host used, the TDFAs can be classified into silica host-based TDFA and ZBLAN based TDFA. Silica host-based TDFA has the limitation of high phonon energy of thulium in silica host, which limits its efficiency. On the other hand, ZBLAN TDFA is relatively efficient, but it also has some limitations, a few of those are chemically instability, difficult manufacturing, the inability of fusion splicing with standard single-mode fiber, high cost, and toxic nature. However, the silica-based TDFA can be easily spliced with the conventional single-mode fiber (SMF) made of silica. For making silica-based TDFA a practical solution, it is desired that the gain of silica TDFA should be improved while maintaining its ability to remain fusion splice ready with silica SMF. The alumina co-doped TDFA with an enhanced $^3H_4$ lifetime of 58 µs is the practical choice over the pure silica fiber. Because it not only enhances the gain but also remains fusion splice ready with the single-mode fiber [8]. Following is the literature related to the S-band amplification by TDFA.

Emmanuel Desurvire (1994) explained the detailed development history of different optical amplifiers [9]. S. D. Jackson et al. (1998) presented continuous-wave lasers based on the silica host thulium holmium co-doped fiber and thulium holmium ZBLAN fiber. They mentioned that the 1064 nm pumping of TDFA is efficient for emission in near 2 µm region [10]. Tetsuro Komukai et al. reported ZBLAN glass host-based TDFA working in the 1470 nm region with a gain of the order of 10 dB in the wavelength region of 1440 nm to 1510 nm. They concluded that the single pumping schemes with a pump wavelength of 676 nm, 790 nm, and 800 nm are inefficient in ZBLAN TDFA [11]. Brian cole et al. (2001) presented the gain behavior of silica-based TDFA. With the 1047 nm pumping (750 mW) and 1410 nm (1100 mW), they observed the gain of around 8 dB with the total pump power of 1850 mW [12]. M. M. Kozak et al. (2004) highlighted that the fusion splicing of ZBLAN TDFA with silica fibers is not possible due to different processing temperatures [13]. Emami S. D. et al. (2014) reported the gain improvement of the order of 5dB in S-band with the macro bending of photonic crystal fiber. The host considered was silica-based alumina co-doped TDFA. However, PCF is costly as its fabrication is difficult as compared to the ordinary TDFA [14]. Z.Li et al. (2015) presented silica host TDFA for a working wavelength range of 1650 nm to 1700 nm. A significant small-signal gain of 29 dB is observed with 1565 nm pumping [15]. Y. Jung et al. (2016) presented a similar silica host-based TDFA for wavelengths exceeding 1650 nm. The peak gain of 35 dB was observed with a low noise figure of around 4.5 dB [16]. It has been observed From the literature that many TDFA amplifier configurations and pumping configurations have been reported in the past by the researchers. Following are the some pumping schemes for TDFA: 1056 nm + 790 nm [13],1565 nm [15], 1060 nm [17]–[19], 1060 nm + 800 nm [20], 1400 nm + 800 nm [21], 1050 nm + 800 nm [22], 1064 nm [23]–[27], 1400 nm + 1560 nm [28], 1050 nm

[29], 1050 nm+1400 nm+800 nm [30]–[32], 690 nm+1400 nm [33].

In our past works, we have analyzed the effect of doping parameters on the silica-based TDFA with $^3H_4$ lifetime of 45μs, and it was observed that the doping parameters have a significant effect on the gain of TDFA [31], [32], [34]. In this present work, the effect of change in the doping concentration and doping radius on the gain of silica host-based TDFA with an enhanced $^3H_4$ lifetime of 58μs has been evaluated. The gain evaluation is carried out using Optisystem 13.0 software for the variation of doping radius (0.3 μm to 1.3 μm) and doping concentration (20×10^{24} m^{-3} and 40×10^{24} m^{-3}) using Optisystem 13.0 simulation software. The Optisystem software is a graphical user interface based optical simulation tool, and it is used for easy and fast simulations. For pumping of TDFA, four pumping schemes of 1050 nm, 1050 nm +1400 nm,1050 nm + 800 nm and 1050 nm +1400 nm + 800 nm pumping are used. The paper is organized into five sections. The introduction and literature review are presented in the first section. The theoretical introduction of TDFA is given in the second section. The third section contains the simulation model and the parameters of TDFA. The results and discussions are carried out in the fourth section of the paper. The conclusions from the evaluated results have been made in section 5. At the end of the paper, a list of references is added.

2. Theory

Thulium doped fiber amplifier is a doped fiber in which thulium atoms are added for S-band amplification. The working principle of TDFA is similar to the EDFA, but the pumping in the case of TDFA is difficult as compared to EDFA. The reason is that many transitions take place in TDFA, and it becomes a 4 level system. The $^3H_4$ level lifetime is not sufficiently high for silica TDFA, and competing transitions result in a lower gain of TDFA. The energy levels of thulium are labeled as $^3H_6, ^3F_4, ^3H_4, ^3F_2, ^3F_3, ^1G_4$. The levels $^3F_2$ and $^3F_3$ are close to each other, and due to minimal energy difference, these levels can be assumed as a single merged level. It is assumed that all the ions are at the $^3H_6$ before pumping, which is the ground state level. For simplicity, the levels are labeled as level 1 to level 5, as shown in Fig. 1.

Fig. 1 shows the mechanism of the pumping of TDFA. The pump of 800 nm directly raises the electrons from the ground state level to level 3. TDFA absorbs the pump signal of 1050 nm for three transitions, which are ground level to level 2, level 1 to level 4, and level 3 to level 5. The third pump of 1400 nm wavelength gets absorbed for transitions between level 0 to level 1 and from level 1 to level 3.
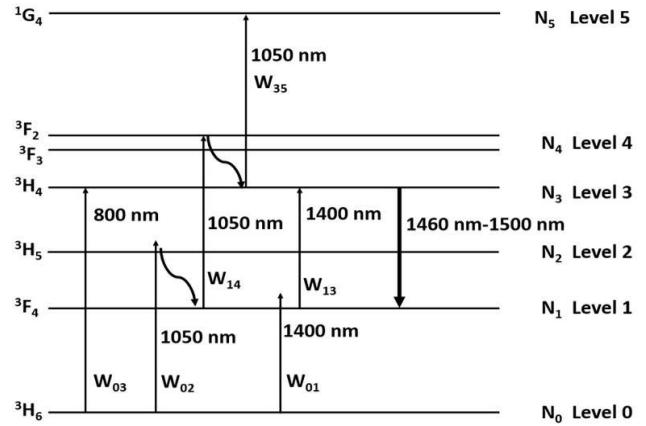

Fig. 1. Energy level diagram for triple pumping [31]

The transition between different levels of TDFA can be categorized into five parts, which are pumping transitions, non-radiative transitions, radiative transitions, amplified spontaneous emission (ASE) transitions, and signal transitions. The atoms at the ground state migrate to higher levels by absorbing the pumps. The rate equations for the different energy levels can be written as

$$\frac{dN1}{dt} = N0.(W01 + W02) - N1.(W10 + W13 + W14 + Anr1 + A10) + N3.(W31 + W32 + Anr3 + A32) + N5.(A51 + A52)$$

$$\frac{dN3}{dt} = N0.(W03) + N1.(W13 + W14) - N3.(W35 + W32 + W31 + W30 + Anr1 + A32 + A31 + A30) + N5.(Anr5 + A54 + A53)$$

$$\frac{dN5}{dt} = N0.(W05) + N3.(W35) - N5.(W50 + Anr5 + A54 + A53 + A52 + A50)$$

And Nt=N0+N1+N3+N5

These rate equations are based on the work of P.Peterka et al. [35]. The TDFA simulation model in Optisystem software is also based on these rate equations. The term N_t is the total electron density. The individual population densities for $_3H^6, _3F^4, _3H^4, _1G^4$ levels are given by parameters $N_0, N_1, N_3,$ and $N_5.$ The stimulated absorption rates and emission rates are defined for the transition between ith level to jth level by term W_{ij}. Similarly, the radiative and non-radiative decay rates from ith level to jth level are symbolized by A_{ij} and A_{nrj} respectively. The non-radiative transitions are responsible for downwards transitions that do not emit energy in the form of photons. With these transitions, the electrons move quickly from level 2 to level 1, and from level 4 to level 3, this is because the radiative rate A_{nr2} and A_{nr4} are very large. This is the reason why the population at level 2 and level 4 are neglected in the modeling. Only $A_{nr1}, A_{nr3}, A_{nr5}$ are considered. The values of radiative and non-radiative lifetimes, along with other parameters of TDFA, are given in Table 1.

Table 1. Simulation parameters

Parameter	Value	Units
Length	8.1	m
Numerical aperture	0.4	-
Core Radius	1.3	μm
Core doping radius	0.3-1.3	μm
Non radiative lifetime 1	20×10^{24}-80×10^{24}	Seconds
Non radiative lifetime 3	0.00043 [19], [21], [26]	Seconds
Non radiative lifetime 5	58e-006 [19], [21], [26]	Seconds
Ar10	0.00054 [19], [21], [26]	1/seconds
Ar30	285.7 [35]	1/seconds
Ar31	1353.85 [35]	1/seconds
Ar32	138.46 [35]	1/seconds
Ar50	46.153 [35]	1/seconds
Ar51	581.4 [35]	1/seconds
Ar52	69.767 [35]	1/seconds
Ar53	348.84 [35]	1/seconds
Ar54	127.91 [35]	1/seconds

The expression for any transition rate W_{ij} from i^{th} level to j^{th} level is given below [35].

$$W_{ij}(z) = \int_0^\infty \frac{\sigma_v(v)}{h.v} . I(z,v).dv$$

where $I(z,v) = i(r,\emptyset,v).P_k(z)$

Here h is the Planck's constant, v is the signal frequency, σ_v is the transition cross-section, and the term 'I' represents light intensity.

The normalized optical intensity for k^{th} beam is defined as P_k, and the propagation equation can be written as.

$$\frac{dP_k}{dz} = u_k.P_k(z).\sum_{ij}^{(10,30,31.50)} \int_0^{2\pi} \int_0^\infty \left(\sigma_{ij}(v_k).N_i(r,\emptyset,z) - \sigma_{ji}(v_k).N_j(r,\emptyset,z) \right).i_k(r,\emptyset).r.dr.d\emptyset -$$
$$u_k.P_k(z).\sum_{ij}^{(02,14,35)} \int_0^{2\pi} \int_0^\infty \left(\sigma_{ji}(v_k).N_i(r,\emptyset,z) \right).i_k(r,\emptyset).r.dr.d\emptyset +$$
$$u_k.P_{0k} \sum_{ij}^{(10,30,31.50)} \int_0^{2\pi} \int_0^\infty \left(\sigma_{ij}(v_k).N_i(r,\emptyset,z).i_k(r,\emptyset).r.dr.d\emptyset - \alpha(v_k).u_k.P_k(z) \right)$$ [35].

Here, the u_k defines the direction of flow of signal and it is +1 for forwarding propagating waves, it is -1 for backward propagating waves. The term P_{0k} is the spontaneous emission contribution from the local population N_i. The term $W_{ij}(z)$ represents the rate of absorption or emission from i^{th} to j^{th} level for any distance value z; it is defined by P. Pterka et al. [35].

$$W_{ij}(z) = \int_0^\infty \lambda \Gamma(\lambda).\sigma_{ij}(\lambda) \frac{\left(P_\lambda^+(z,\lambda) + P_\lambda^-(z,\lambda) \right)}{hc\pi b^2} d\lambda$$
$$\text{where} \quad \Gamma(\lambda) = \frac{\int_0^\infty |E(r,\emptyset,\lambda)|^2 N(r).r.dr}{N_t \int_0^\infty |E(r,\emptyset,\lambda)|^2 .r.dr}$$

The term $\Gamma(\lambda)$ is the overlap integral.
P. Peterka et al. [35] proposed the propagation equation of the beams through the doped fiber, which is given by.

$$\frac{dP^+(\lambda)}{dz} = \Gamma(\lambda).P^+(\lambda).\sum_{ij}^{(10,30,31.50,32)} \left(N_i.\sigma_{ij}(\lambda). - N_j.\sigma_{ij}(\lambda) \right) - \Gamma(\lambda).P^+(\lambda).\left(N_0.\sigma_{02}(\lambda) + N_1\sigma_{14}(\lambda) + N_3\sigma_{35}(\lambda) \right) + \Gamma(\lambda).\sum_{ij}^{(10,30,31,50,32)} 2hv_{ij}\Delta v \, N_i.\sigma_{ij}(\lambda) - \alpha(\lambda).P^+(\lambda)$$

The same propagation equation is used in the TDFA model in the Optiysem simulation software. For the steady-state analysis, the equations of time derivatives $\frac{dN1}{dt}$, $\frac{dN3}{dt}$, $\frac{dN5}{dt}$ are equated to zero. By this, the problem reduces to the steady-state. With the specified boundary conditions at z = 0 and z = L, the equations are integrated over space and frequency. By comparing the input power and output power, the gain is obtained.
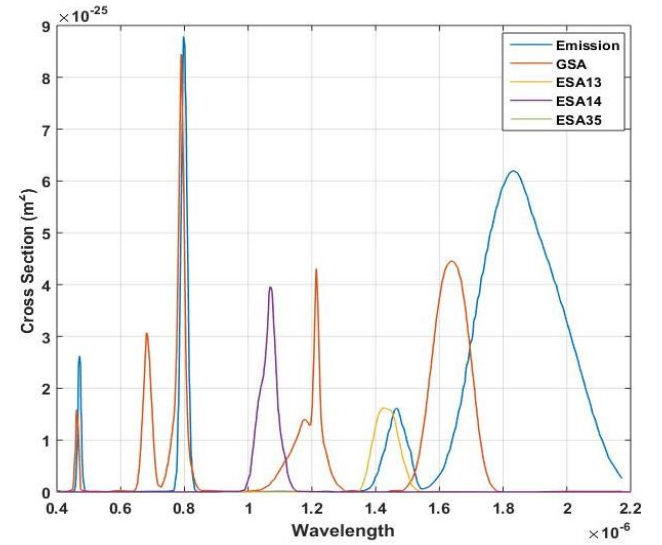

Fig. 2. Absorption and emission cross-section spectra of thulium [26], [35] *(color online)*

In Fig. 2, the ground state absorption (GSA), Excited-state absorption ESA13 (level 1 to level 3), ESA14 (level 1 to level 4), ESA35 (level 3 to level 5) and emission cross-sections have been plotted.

3. Simulation setup

The simulation setup used for the analysis is shown in Fig. 3. In the present work, four pumping cases have been considered, which are 1050 nm, 1050 nm+1400 nm, 1050 nm+800 nm, and 1050 nm+1400 nm+800 nm. The signals from 1460 nm to 1520 nm with 5 nm channel spacing and -20dB power each are generated by continuous wave laser array. The signals are multiplexed together and are supplied to the input of TDFA. The scheme of pumping applied to the TDFA is also shown in Fig. 3. A total of three pumps of 1050 nm, 1400 nm, and 800 nm are applied to TDFA. The pump power of the 1050 nm pump is fixed to 1000 mW in all the cases. However, the pump power of the auxiliary pump of 1400 nm or 800 nm is fixed to 300 mW if applicable.
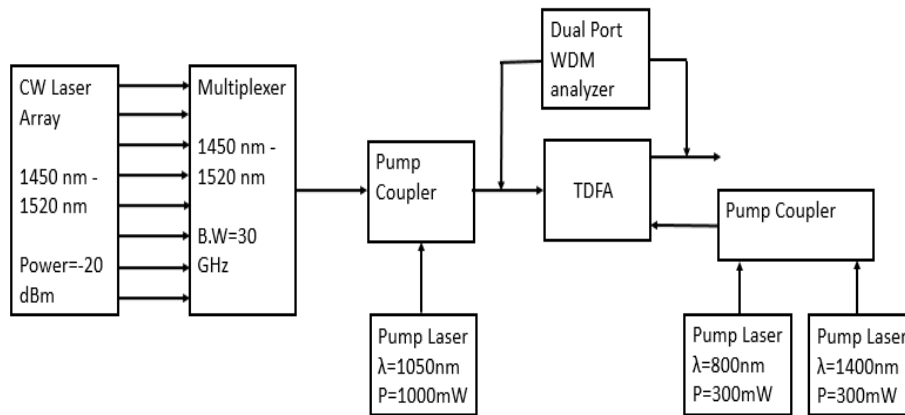
Fig. 3. Simulation setup

4. Results and discussion

The gain of the TDFA is evaluated for four pumping cases, which are single pumping of 1050 nm, dual pumping schemes of 1050 nm + 1400 nm, or 1050 nm + 800 nm, and triple pumping of 1050 nm + 1400 nm + 800 nm. The results for the 1470 nm signal wavelength are plotted for the variation of doping radius and varied different doping concentrations. The gain curves for the 1460 nm to 1520 nm are also plotted for every pumping scheme. The results are discussion is presented in the following sections.

4.1. Results for the 1050nm pumping of the TDFA

The effect of doping radius and doping concentration for a 1050 nm pump on the TDFA with 58 μs $^3H_4$ lifetime has been shown in Fig. 4.
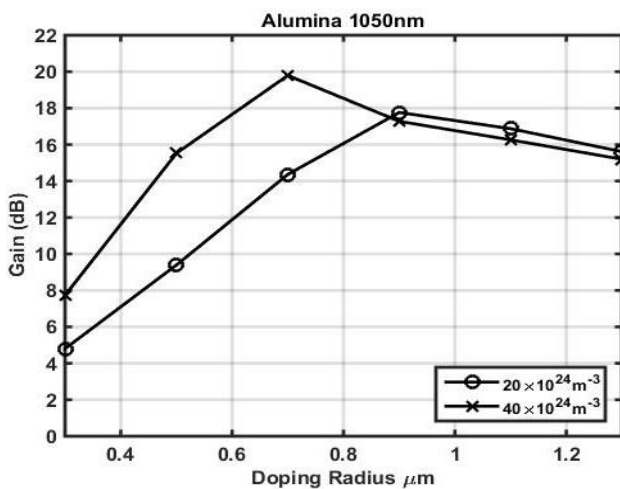
Fig. 4. Effect of doping radius and doping concentration on the gain to 1470 nm in TDFA pumped by 1050 nm

For a doping concentration of 20×10^{24} m^{-3}, the doping radius of 0.9 μm results in a gain of 17.76 dB. In this case, the gain enhancement of 2.5 dB is observed over the gain for a 1.3 μm doping radius. The gain increases to 19.8 dB for 40×10^{24} m^{-3} concentration and the doping radius 0.7μm. Here, the gain enhancement of ~4dB over the gain of TDFA with 1.3 μm is observed. It is seen from the figure that the gain increases as the doping radius decreases from 1.3 μm. However, after attaining maximum gain for a particular doping concentration, the gain decreases sharply with more decrease in the doping radius.
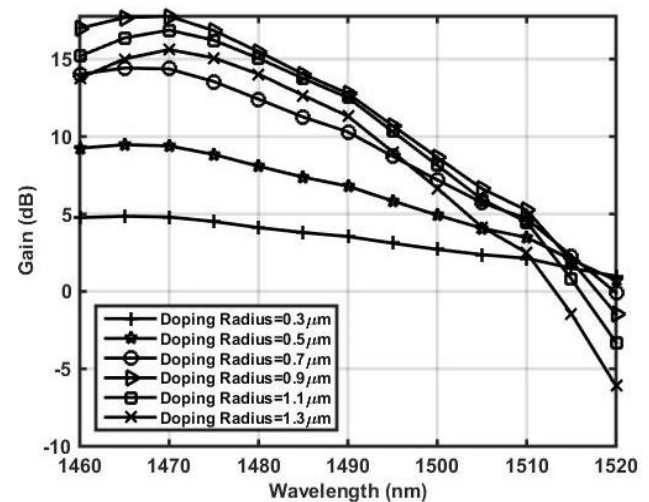

Fig. 5. Effect of doping radius on the gain of TDFA with a doping concentration of 20×10^{24} m^{-3} and 1050 nm pumping

Fig. 5 shows the gain for the 1050 nm pumping of 20×10^{24} m^{-3} doped TDFA. This configuration provides the best gain curve (17.76 dB peak at 1470 nm) for a doping radius of 0.9 μm.
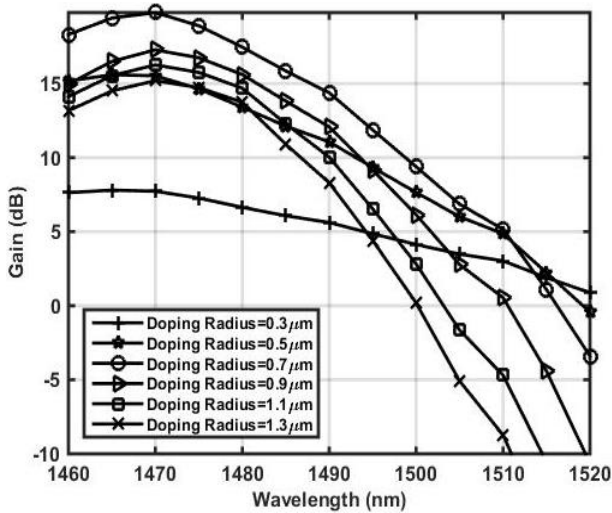
Fig. 6. Effect of doping radius on the gain of TDFA with a doping concentration of $40 \times 10^{24} m^{-3}$ and 1050nm pumping

The best gain curve with a peak gain of 19.8 dB for the 40×10^{24} m^{-3} doping concentration and 1050 nm pumping is found for a 0.7 µm doping radius, which is shown in Fig. 6.

4.2. Results for 10% alumina co-doped silica TDFA with   1050 nm + 800 nm pumping

The gain of TDFA for the addition of an 800 nm auxiliary pump with the main pump of 1050 nm is shown in Fig. 7 and Fig. 10, respectively. The gain does not improve with the addition of an auxiliary pump for a doping concentration of 20×10^{24} m^{-3}, and the gain of 16.3 dB gain is observed for the doping radius 1.3 µm. The maximum gain among all of 21.77 dB for 40×10^{24} m^{-3} is observed for the doping radius of 0.9 µm.
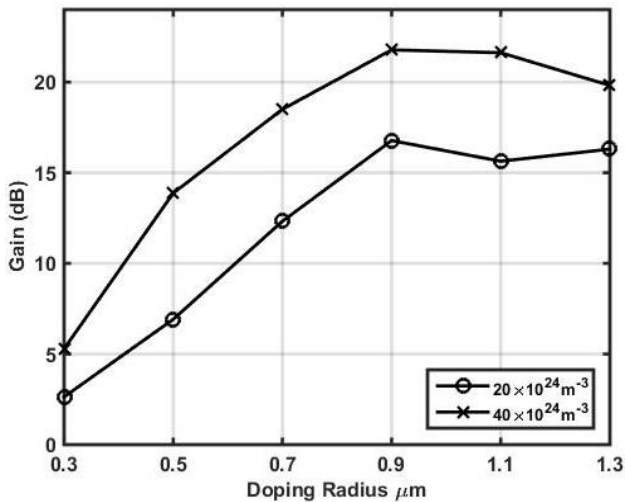

Fig. 7. Effect of doping radius and doping concentration on the gain to 1470nm in TDFA pumped by 1050 nm + 800 nm

Fig. 7 shows the gain variation in 1460 nm to 1520 nm for the 1050 nm + 800 nm pumping. No gain enhancement is seen; the gain does not increase for different doping radius and 20×10^{24} m^{-3} doping concentration case. The gain of 16.77 dB and 16.3 dB for 0.9 µm and 1.3 µm doping radius, respectively, are found.

However, the gain enhancement is seen for doping concentration of 40×10^{24} m^{-3} (0.9 µm) over 20×10^{24} m^{-3} (1.3 µm). By considering practicality and gain flatness it can be stated that the most suitable gain curves are observed for 20×10^{24} m^{-3} (0.9 µm), 40×10^{24} m^{-3} (0.9 µm).
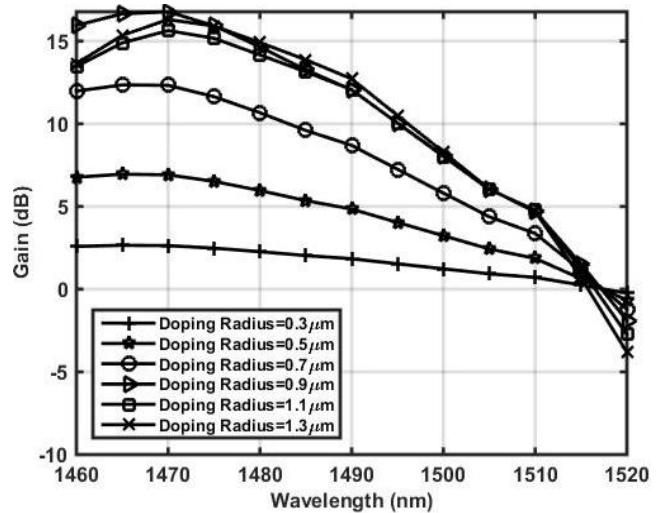

Fig. 8. Effect of doping radius on the gain of TDFA with a doping concentration of 20×10^{24} m^{-3} and 1050 nm + 800 nm pumping

From Fig. 8, it is clear that the 0.9 µm-1.3 µm doping radius provides almost the same gain for wavelengths 1470 nm to 1510 nm for 1050 nm + 800 nm pumping. The gain at 1460 nm is highest for the 0.9 µm doping radius. The gain values of 15.94 dB, 16.77 dB, and 1.51 dB have been observed for the 1460 nm,1470 nm, and 1515 nm.

For the 1050 nm + 800 nm pumping of TDFA doped with 40×10^{24} m^{-3} doping concentration, the gain curves are shown in Fig. 9. Here 21.7 dB peak gain at 1470 nm is observed for both 0.9 µm and 1.1µm doping radius values. However, for wavelengths exceeding 1480 nm, the gain for the 1.1 µm is lower than the gain for the 0.9 µm doping radius, The peak gain of 19.8dB has been observed for 1470 nm wavelength.
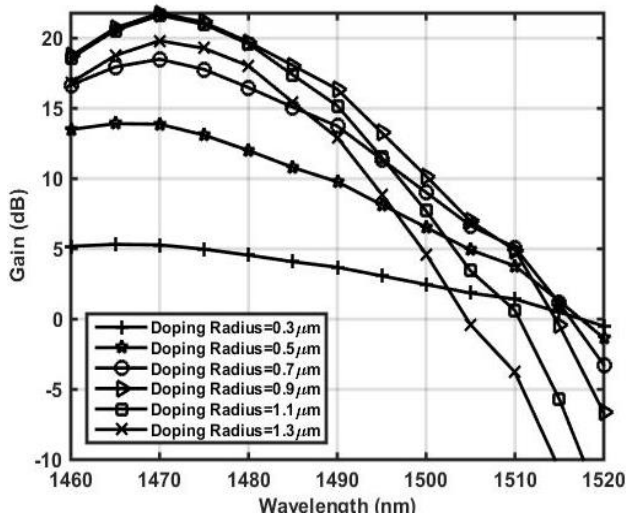
Fig. 9. Effect of doping radius on the gain of TDFA
with a doping concentration of 40×10^{24} m^{-3} and
1050 nm + 80 0nm pumping

4.3. Results for 10% alumina co-doped silica
TDFA with 1050 nm + 1400 nm pumping

The gain curves for the dual pumping of 1050 nm + 1400 nm is shown in Fig. 10. Almost no gain enhancement for the 20×10^{24} m^{-3} doping concentration is seen in this case. The maximum gain of 20 dB is observed at 1.3 µm. However, for the 40×10^{24} m^{-3} (0.9 µm). The gain peak of 25 dB has been observed. Also, It is observed that the gain peak shifts to lower doing radius values as the doping concentration increases.
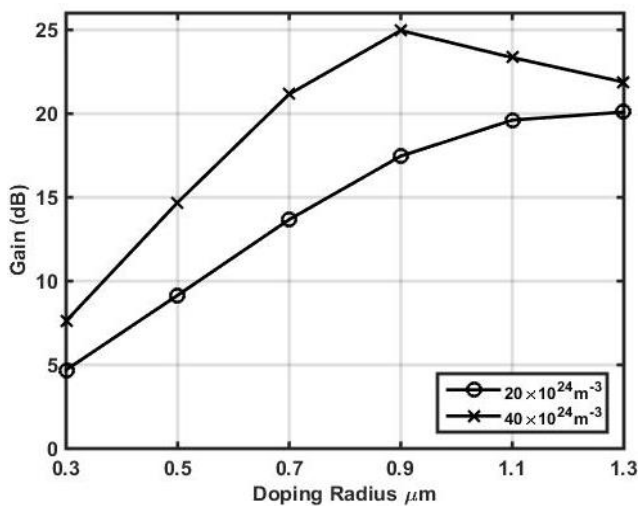

Fig. 10. Effect of doping radius and doping concentration on
the gain to 1470 nm in TDFA pumped by 1050 nm +1400 nm

From Fig. 11, it is observed that the maximum gain is found for the 1.3 µm doping radius for a doping concentration of 20×10^{24} m^{-3}. However, the peak gain of 25 dB is found for the 40×10^{24} m^{-3} doping concentration. Fig. 11 is showing the gain TDFA doped with a doping concentration of 20×10^{24} m^{-3} and 1050 nm + 1400 nm

pumping. Here the gain curves for the 1.3 µm and 1.1 µm are almost similar to the peak gain of ~20 dB for 1470 nm.

Fig. 12 shows the gain of TDFA pumped with 1050 nm + 1400 nm for the 40×10^{24} m^{-3} thulium concentration.

For the 1470 nm signal, the peak gain is 25 dB for a doping radius of 0.9 µm. The gain for all wavelengths decreases as the doping radius increases beyond 0.9 µm. For the doping radius of 1.3 µm, 21.9 dB peak gain is observed. However, in this case, the gain decreases sharply as the wavelength increases; the gain is positive only up to 1500 nm.
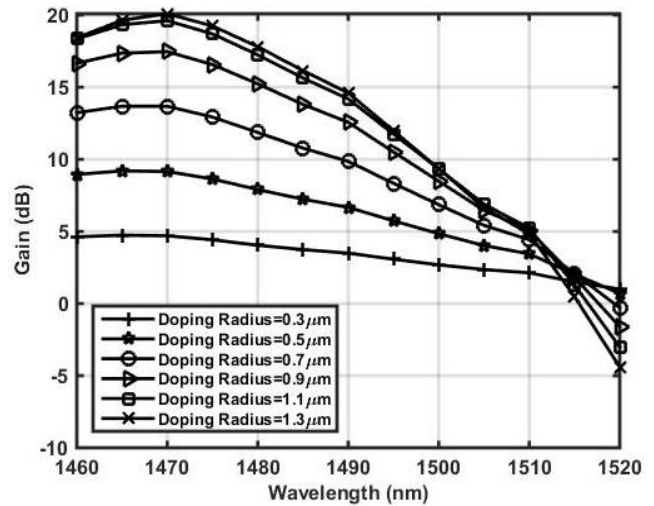

Fig. 11. Effect of doping radius on the gain of TDFA
with a doping concentration of 20×10^{24} m^{-3} and
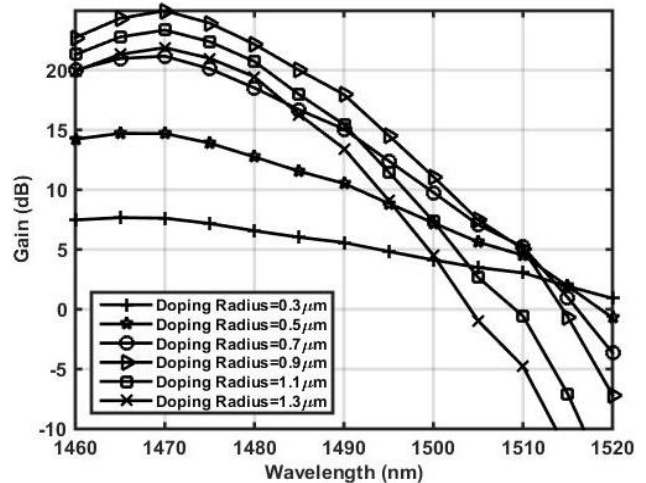*1050 nm +1400 nm pumping*

Fig. 12. Effect of doping radius on the gain of TDFA
with a doping concentration of 40×10^{24} m^{-3} and
1050 nm +1400 nm pumping

4.4. Results for 10% alumina co-doped silica
TDFA with 1050 nm + 1400 nm + 800 nm
Pumping

Fig. 13 shows the gain curves for the 1050 nm + 1400 nm + 800 nm pumping of TDFA. For 1050 nm + 1400 nm

+ 800 nm pumping, the gain does not increase for a doping concentration of 20×10^{24} m^{-3}. From Fig. 13, a gain of 20.4 dB is observed for a 1.3 μm doping radius. In this case, the highest gain of ~30 dB is obtained for the doping concentration of 40×10^{24} m^{-3} and a doping radius of 1.1 μm. Here, the gain enhancement is ~15 dB over the gain of TDFA with a doping concentration of 20×10^{24} m^{-3} (1.3 μm) and 1050 nm pumping.

Fig. 15 shows the gain for 40×10^{24} m^{-3} doping concentration. The doping radius of 1.1 μm with 40×10^{24} m^{-3} doping concentration provides 29.5 dB gain. The gain for the 1.3 μm doping radius is lower than the gain observed for the 1.1 μm in the whole wavelength range.
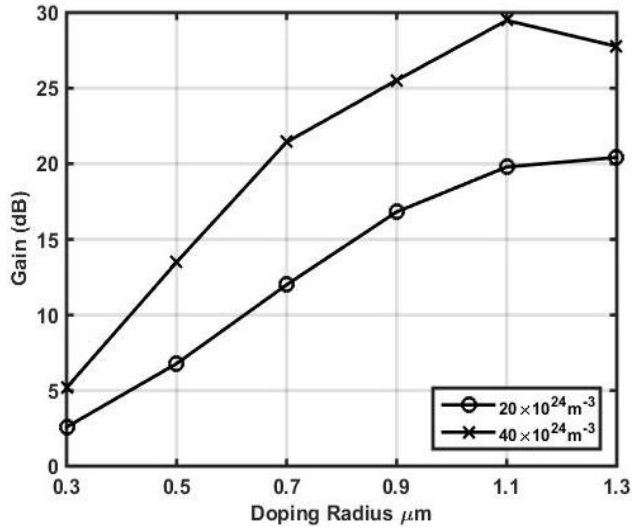

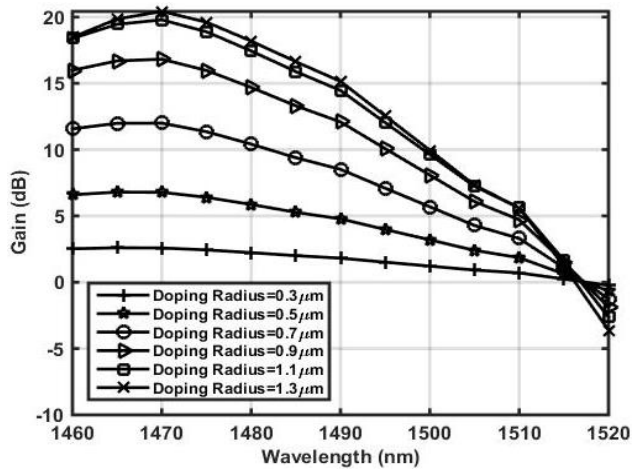*Fig. 13. Effect of doping radius and doping concentration on the gain to 1470nm in TDFA pumped by 1050 nm + 1400 nm + 800 nm*

Fig. 15. Effect of doping radius on the gain of TDFA with a doping concentration of 40×10^{24} m^{-3} and 1050 nm + 1400 nm + 800 nm pumping

The best and the flat gain curve is obtained in the case of the 20×10^{24} m doping concentration and 1.3 μm doping radius, as shown in Fig. 14. Here, the gain for the 1.1 μm and 1.3 μm doping radius values is almost with less than 1 dB variation.

In Fig. 16, the important gain curves found after the analysis are plotted for their comparison. While selecting the best cases, the minimum possible doping concentration and maximum possible doping radius values are preferred. Becausefarication would be easy for a higher doping radius, and TDFA with a low doping radius dissipated less heat during operation.

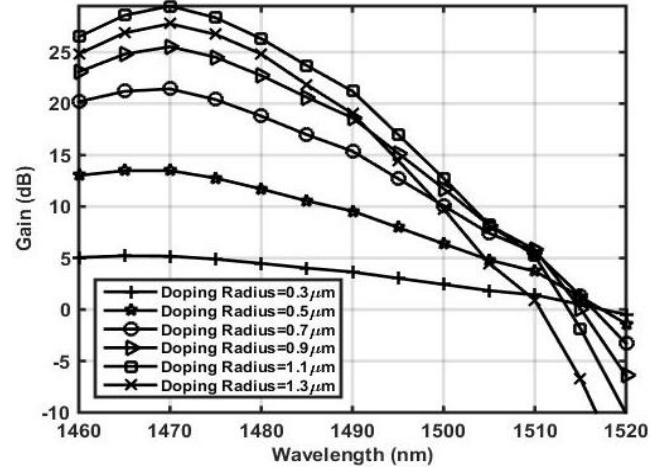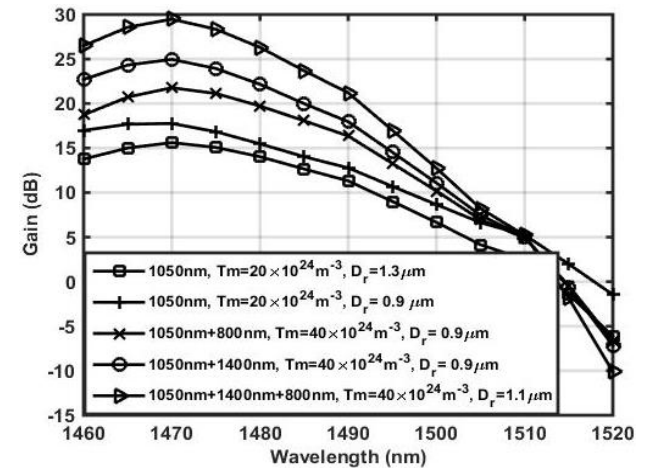*Fig. 14. Effect of doping radius on the gain of TDFA with a doping concentration of 20×10^{24} m^{-3} and 1050 nm + 1400 nm + 800 nm pumping*

Fig. 16. Gain comparison of important cases found for the 10% alumina co-doped TDFA

The TDFA with a doping concentration of 20×10^{24} m^{-3} and oping radius of 1.3 μm while pumped by 1050 nm pump can be considered as the reference case. Here, the peak gain observed is ~15 dB at 1470 nm. But this gain is lowest among all the plotted curves. The gain

enhancement of 2.75 dB is observed for the same pumping of 1050 nm by reducing the doping radius to 0.9 µm from 1.3 µm. The dual pumping schemes of 1050 nm + 1400 nm and 1050 nm + 800 nm performs better than the 1050 nm pumping. The dual pumping schemes of 1050 nm + 800 nm and 1050 nm +1400 nm provide the gain peaks of 21.77dB and 25 dB, respectively, The gain for both the cases is ~5 dB at 1510 nm.

The maximum gain enhancement of ~15 dB over the typical case is observed for the 1050 nm + 1400 nm + 800 nm pumping with the TDFA doping concentration of $40{\times}10^{24}$ m^{-3} and doping radius of 1.1 µm. Here, the maximum gain of 29.5 dB is observed at 1470 nm. Also, the gain exceeds 25 dB in 1460 nm to 1480 nm wavelength region.

5. Conclusion

From the results, it can be concluded that the 1050 nm + 1400 nm pumping shows improvement in the gain over both the single 1050 nm pumping and 1050 nm + 800 nm dual pumping. However, 1050 nm + 1400 nm + 800 nm produces the highest gain among all the cases without exception.

Out of the dual pumping schemes, the pumping of 1050 nm + 1400 nm outperforms the 1050 nm + 800 nm pumping. Therefore, for dual pumping, 1050 nm + 1400 nm pumping is preferable over 1050 nm + 800 nm. Also, it has been observed that for every pumping case, as the doping concentration increases, the peak shifts towards lower doping radius values. The 1050 nm + 1400 nm + 800 nm pumping of the TDFA results in the peak gain of ~30 dB for the optimum parameter of $40{\times}10^{24}$ m^{-3} doping concentration and 1.1 µm doping radius. The presented optimum parameters provide a significant gain enhancement ~15 dB over the reference case of 1050 nm pumping of TDFA with a doping concentration of $20{\times}10^{24}$ m^{-3} and a doping radius of 1.3 µm.

References

[1] S. Singh, R. S. Kaler, Opt. Eng. **54**(10), 100901_1 (2015).
[2] S. Singh, R. S. Kaler, Opt. Laser Technol. **68**, 89 (2015).
[3] D. Malik, K. Pahwa, A. Wason, Optik **127**(23), 11131 (2016).
[4] S. Singh, A. Singh, R. S. Kaler, Optik **124**(2), 95 (2013).
[5] S. Bhaskar, M. L. Sharma, R. Kaur, Int. J. Adv. Comput. Sci. Appl. Spec. Issue Wirel. Mob. Networks. **1**(2), 19 (2011).
[6] R. Kaur, R. Randhawa, R. S. Kaler, Opt. - Int. J. Light Electron Opt. **124**(8), 693 (2013).
[7] R. Goyal, M. Rani, S. Dewra, J. Telecommun. Switch. Syst. Networks **3**, 1 (2016).
[8] P. Peterka et al., Proc. SPIE 7843, High-Power Lasers and Applications V. **7843,** 78430A-1 (2010).
[9] E. Desurvire, Physics Today **47**(1), 20 (1994).
[10] S. D. Jackson, T. A. King, IEEE J. Quantum Electron. **34**(9), 1578 (1998).
[11] T. Komukai, T. Yamamoto, O. Sugawa, Y. Miyajima, IEEE J. Quantum Electron. **31**(11) 1880 (1995).
[12] B. Cole, M. L. Dennis, Optical Fiber Communication Conference and Exhibit, Anaheim, CA, 2001, pp. TuQ3-1-TuQ3-3.
[13] M. M. Kozak, R. Caspary, W. Kowalsky, Proceedings of 6th International Conference on Transparent Optical Networks. **2**, 51 (2004).
[14] S. D. Emami, A. R. Muhammad, S. W. Harun, H. Ahmad, H. A. A. Rashid, Optical Fiber Communications Conference and Exhibition (OFC), 2014, San Francisco, CA **1**, 14 (2014).
[15] Z. Li et al., 2015 Optical Fiber Communications Conference and Exhibition (OFC), Los Angeles, CA **6**, 1 (2015).
[16] Y. Jung et al., Opt. Soc. Am. M3D, M3D5 (2016).
[17] J. M. Thomas, D. Crippa, A. Maroney, Optical Fiber Communication Conference and Exhibit, 2001. OFC 2001, Anaheim, CA, 2001, pp. WDD9-1-WDD9-3.
[18] P. R. Watekar, S. Ju, W. Han, OFC/NFOEC Technical Digest. Optical Fiber Communication Conference **3**, 3 (2005).
[19] W. Blanc et al., Proceedings of SPIE - The International Society for Optical Engineering, **6180**, 61800V-1, 2006.
[20] S. Luthi, M. Sundheimer, W. Margulis, A. S. Gomes, Electron. Lett. **41**(25), 7 (2005).
[21] P. Peterka et al., Opt. Mater. **30**(1), 174 (2007).
[22] A. Gomes, M. Carvalho, M. Sundheimer, C. Bastos-Filho, J. Martins-Filho, W. Margulis, OFC 2003 Optical Fiber Communications Conference **2**, 632 (2003).
[23] P. R. Watekar, S. Ju, an W. Han, IEEE Photonics Technol. Lett. **18**(19), 2035 (2006).
[24] J. Chang, Q. Wang, G. Peng, Opt. Mater. **28**, 1088 (2006).
[25] P. R. Watekar, S. Ju, W. T. Han, J. Light. Technol. **25**(4), 1045 (2007).
[26] P. Peterka, I. Kasik, A. Dhar, B. Dussardier, W. Blanc, Opt. Express **19**(3), 2773 (2011).
[27] F. I. El-nahal, A. H. M. Husein, Open J. Appl. Sci. **2**(4B), 5 (2012).
[28] T. Kasamatsu, Y. Yano, T. Ono, IEEE Photonics Technol. Lett. **13**(5), 433 (2001).
[29] P. Peterka et al., Opt. Mater. **30**(1), 174 (2007).
[30] R. Singh, M. L. Singh, B. Kaur, Optik **123**(20), 1815 (2012).
[31] R. Singh, M. L. Singh, Optoelectron. Adv. Mat. **10**(9–10), 619 (2016).
[32] R. Singh, M. L. Singh, 2016 International Conference

on Recent Advances and Innovations in Engineering, ICRAIE 2016, 2017.

[33] M. Nix, S. S. Yam, 19th Annual Meeting of the IEEE Lasers and Electro-Optics Society, Montreal, 390 (2006).

[34] R. Singh, M. L. Singh, Optik **140**, 65(2017).

[35] P. Peterka, B. Faure, W. Blanc, M. Karasek, B. Dussardier, Opt. Quantum Electron. **36**, 201 (2004).

_____
*Corresponding author: rajandeep1987@gmail.com
mlsingh7@gmail.com